

# Nanoscale, Electric Field-Driven Water Bridges in Vacuum Gaps and Lipid Bilayers

Ming-Chak Ho · Zachary A. Levine ·  
P. Thomas Vernier

Received: 10 January 2013 / Accepted: 17 April 2013 / Published online: 5 May 2013  
© Springer Science+Business Media New York 2013

**Abstract** Formation of a water bridge across the lipid bilayer is the first stage of pore formation in molecular dynamic (MD) simulations of electroporation, suggesting that the intrusion of individual water molecules into the membrane interior is the initiation event in a sequence that leads to the formation of a conductive membrane pore. To delineate more clearly the role of water in membrane permeabilization, we conducted extensive MD simulations of water bridge formation, stabilization, and collapse in palmitoylcholine bilayers and in water–vacuum–water systems, in which two groups of water molecules are separated by a 2.8 nm vacuum gap, a simple analog of a phospholipid bilayer. Certain features, such as the exponential decrease in water bridge initiation time with increased external electric field, are similar in both systems. Other features, such as the relationship between water bridge lifetime and the diameter of the water bridge, are quite different between the two systems. Data such as these contribute to a better and more quantitative understanding of the relative roles of water and lipid in membrane electropore creation and annihilation, facilitating a mechanism-driven development of electroporation protocols. These methods can be extended to more complex, heterogeneous systems that include membrane proteins and intracellular and extracellular membrane attachments,

leading to more accurate models of living cells in electric fields.

**Keywords** Electroporation · Electropore · Molecular dynamics · Water bridge · Lipid electropore annihilation

## Introduction

The cell membrane separates the cell interior from the external environment, enabling control of substances traveling into and out of the cell. When a sufficiently high electric field is applied, the cell membrane becomes permeable to charged species and small molecules that normally cannot cross the membrane barrier, a phenomenon known as electroporation, also called electroporation (Zimmermann et al. 1974; Teissie et al. 2005). This nonlethal method for modifying membrane permeability permits the introduction of foreign materials into living cells, enabling applications like electrochemotherapy (Mir et al. 2003) and electric field mediated gene transfer (Heller and Heller 2006). Electroporation (electroporation) has been studied for decades experimentally (Neumann et al. 1982) and theoretically with continuum models (Weaver and Chizmadzhev 1996; Krassowska and Filev 2007). However, a precise characterization of the structures responsible for the increased permeability in living cells has not yet been achieved.

Identifying the constituents of the permeabilized membrane is challenging because of the small dimensions (nanometers) of the putative electropores and the short time scale (nanoseconds) of pore creation, which makes direct observation of electroporation inaccessible to current experimental methods. Given this difficulty, molecular dynamics (MD) simulations have been employed in recent

---

M.-C. Ho (✉) · Z. A. Levine  
Department of Physics and Astronomy, University of Southern  
California, 920 Bloom Walk, SSC 312, Los Angeles,  
CA 90089-0484, USA  
e-mail: mingcho@usc.edu

P. T. Vernier  
Ming Hsieh Department of Electrical Engineering, Viterbi  
School of Engineering, University of Southern California,  
Los Angeles, CA, USA

years for the study of electroporation at the molecular level (Tieleman 2004; Tarek 2005), and they have revealed microscopic aspects of the electroporation of lipid bilayers that are consistent with experiments (Vernier and Ziegler 2007; Böckmann et al. 2008; Fernández et al. 2010; Piggot et al. 2011; Levine and Vernier 2012).

Among the mechanistic molecular details of electroporation that remain to be clarified are the initial steps in the reorganization of water and lipid that leads to the formation of a pore in a lipid bilayer. Previous MD studies have suggested that the intrusion of water molecules into the hydrophobic, phospholipid tail region of the bilayer is the earliest event that can be identified (Tieleman 2004; Vernier and Ziegler 2007). After interfacial water molecules enter into and then bridge the bilayer interior, lipids follow and rearrange to form a hydrophilic wall around the water column.

In an important analytical study, Okuno et al. (2009) demonstrated that under the influence of external electric field, water molecules rearrange themselves (due to their dipole moments) to form an energy-minimized, quasi-conical structure. We observe similar structures in the pore initiation stage in MD simulations of electroporation (Vernier et al. 2013), and we speculate that this energy-minimizing configuration of interfacial water in an electric field normal to the interface is the key initiating structure in the formation of an electropore, which we can consider to be the electric field-mediated construction of a water bridge across a low-permittivity barrier. Here we extend Tieleman's (2004) report of the simulated "electroporation" of octane by comparing the even simpler case, where the low-permittivity gap is a vacuum, to lipid bilayer systems. In this work we examine the dynamics of water bridges in different stages of electroporation in two systems: water–lipid–water (a POPC bilayer sandwiched between two layers of water), and water–vacuum–water (WVW, a vacuum gap between two layers of water). In the absence of an applied electric field, intermolecular attractions (hydrogen bonding) stabilize the bulk water and make the formation of a water bridge across the gap energetically unfavorable. An applied field stabilizes protrusions of water molecules from the interface into the vacuum gap and increases the probability of bridge formation. Although the water–vacuum–water system is somewhat artificial, it is stable on the time scale of our simulations, and it provides a simple view of the dynamics of interfacial water under the influence of an applied electric field.

## Methods

### Molecular Dynamics Simulations

All simulations were performed using GROMACS version 4.0.5 (Hess et al. 2008) on the University of Southern

California High Performance Computing and Communications (HPCC) Linux cluster (<http://www.usc.edu/hpcc/>). Lipid topologies were taken from OPLS united-atom parameters (Berger et al. 1997) and the Simple Point Charge (SPC) model (Berendsen et al. 1981) was used for water. POPC systems were simulated in constant particle number, pressure, temperature (NPT), and constant particle number, volume, temperature (NVT) ensembles, as indicated. The NVT setting was used for WVW systems. Note that WVW systems cannot be sustained in an NPT configuration since the pressure coupling would change the volume of the simulation box, push the water layers together, and collapse the vacuum gap. The temperature was held at 310 K with an external heat bath using a velocity rescaling algorithm (Bussi et al. 2007) with a relaxation time of 0.1 ps. For the NPT ensemble, pressure was held at 1 bar using a weak coupling algorithm (Berendsen et al. 1984), with a relaxation time of 1 ps and compressibility of  $4.5 \times 10^{-5} \text{ bar}^{-1}$  semi-isotropically applied in both normal and in-plane directions relative to the membrane. Bond lengths were constrained using the LINCS algorithm (Hess et al. 1997) for lipids and the SETTLE algorithm (Miyamoto and Kollman 1992) for water. Short-range electrostatic and Lennard-Jones interactions were cut off at 1.0 nm. Long-range electrostatic interactions were calculated with a PME algorithm (Essmann et al. 1995) using fast Fourier transforms and conductive boundary conditions. Reciprocal-space interactions were evaluated on a 0.12 nm grid with fourth order B-spline interpolation. Periodic boundary conditions in all directions were employed to mitigate system size effects.

### Structure

POPC systems contain a lipid bilayer composed of 128 POPC lipids (64 per leaflet) and  $\sim 4,480$  water molecules (35 waters/lipid), with initial system dimensions of  $\sim 7 \text{ nm} \times 7 \text{ nm} \times 7 \text{ nm}$ . WVW systems were created by using a custom Perl script to remove waters from the central region of a volume of bulk water to produce the desired gap sizes. Systems were equilibrated for 300 ps so that both kinetic and potential energies reached a steady value. The planes of the water–lipid interface and the water–vacuum interface are normal to the Z direction of the simulation box.

### Water Bridge Initiation Time, Annihilation Time

Initiation and annihilation times for an electropore in a lipid bilayer system were defined previously (Levine and Vernier 2010), and we establish similar definitions here for water bridge initiation and annihilation times. For both water–lipid–water and water–vacuum–water systems the

water bridge initiation time is defined as the time for the top and bottom water groups to first merge (without subsequently separating) after the application of the external electric field. The water bridge annihilation time is defined as the time for the water to separate into top and bottom groups (without subsequently reconnecting) after the external field is removed.

#### Measurement of Water Bridge Radius

A Perl script is used to measure the radius of the water bridge. The script first obtains the water density profile in  $z$  and defines the water bridge boundaries as the planes where the water density is 50 % of the bulk value. Then the script subdivides the water bridge region into 10 bins (Fig. 1). Within each bin, the script finds the largest and smallest  $x$  coordinate of all the water molecules within the bin,  $x_{\max}$  and  $x_{\min}$ , and the same is done for the  $y$  coordinates. For each bin,  $r_x = (x_{\max} + x_{\min})/2$ ,  $r_y = (y_{\max} + y_{\min})/2$ , and  $r_{\text{bin}} = (r_x + r_y)/2$ . The water bridge radius for a particular time frame is defined as the average of the five smallest values of  $r_{\text{bin}}$  during that time window.

#### Images

Molecular graphics images were generated with Visual Molecular Dynamics (VMD) (Humphrey et al. 1996).

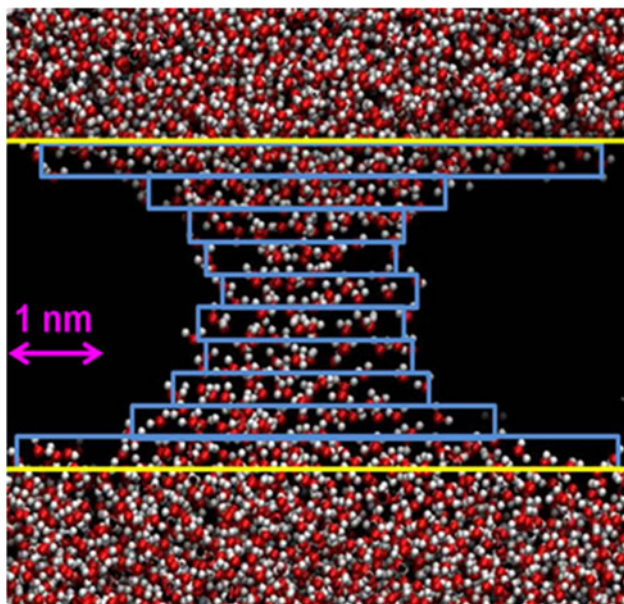


**Fig. 1** Water bridge radius measurement. *White dots* are hydrogen atoms and *red dots* are oxygen atoms of the water molecules. *Yellow lines* are the boundaries of the water bridge region defined by the radius measurement script. *Blue boxes* denote the bins defined by the script with the corresponding  $x_{\max}$  and  $x_{\min}$  values

## Results and Discussion

### Internal Electric Field Versus External Electric Field

We use the magnitude of the electric field in the low-permittivity interior (hydrocarbon chains or vacuum) as a normalizing reference for comparisons between water–lipid–water and water–vacuum–water systems. For a POPC system, the distance between the top and bottom water groups is determined by the properties of the lipid bilayer and does not change more than 15 % over the range of field magnitudes used in this work (Ziegler and Vernier 2008), so the internal electric field for a given POPC system is a function of the applied (external) electric field.

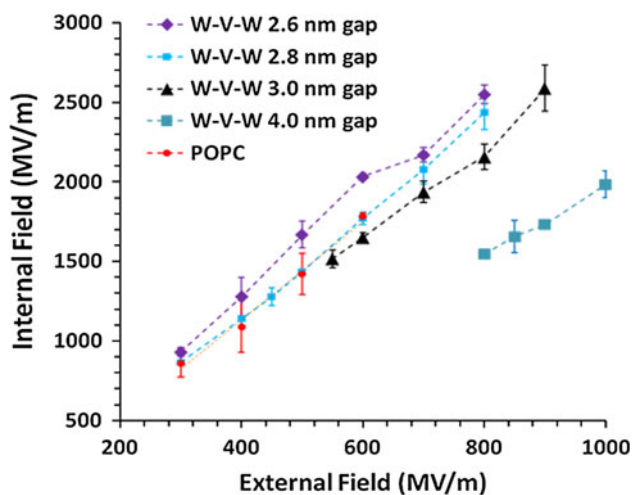
For a WVV system the gap size is arbitrary. Because one component of the internal electric field is generated by the surface charge associated with the water dipoles at the water–vacuum interface, the internal electric field for a given external field will be different for different gap sizes. To permit comparisons of the systems with vacuum (WVV) and lipid (WLW) dielectrics, we selected a vacuum gap for the WVV systems that results in a relation between internal and external electric field that is equivalent to that observed in WLW systems, where the dimensions of the low-permittivity interior are not arbitrary but are determined rather by the properties of the lipid bilayer.

Figure 2 shows the linear relationship between external and internal electric fields for POPC systems and WVV systems with different vacuum gap thicknesses. The internal field is defined as the local field at the center of the system (between the top and bottom water groups), and it is calculated by integrating charge density using the GROMACS function `g_potential`. As mentioned above, for WVV systems the internal field increases when the vacuum gap decreases. The WVV system with a 2.8 nm vacuum gap exhibits an external versus internal field relationship that is very close to that of a POPC system.

### Water Bridge Formation

The dynamics of water bridge formation are similar in POPC and WVV systems (Fig. 3). When an external electric field is applied, water molecular dipoles rotate in the direction of the field, and, after an interval randomly distributed around a time that is dependent on the field strength, an assembly of water molecules begins to intrude into the hydrocarbon interior of the lipid bilayer or the vacuum gap of a WVV system. For WVV systems the initiation time is also a function of the vacuum gap size. In a very short time the chain of water extends from one interface to the other, forming a bridge.

Water bridge initiation times with different external field strengths are given in Fig. 4a. In both systems, WVV



**Fig. 2** Internal versus external electric field in WVW and POPC systems. The internal field is measured at the midpoint between the upper and lower water groups. Each data point is the average of 3 trials. *Error bars* are the standard deviation

and POPC, the initiation time varies with the external field in the form  $\tau = \tau_0 e^{-f(E)}$ , where  $f(E)$  is a function of the field  $E$  that describes the energy barrier for water bridge

creation. In the commonly used continuum models of electroporation, a quadratic dependence on  $E$  is expected for  $f(E)$  (Weaver and Chizmadzhev 1996; DeBruin and Krassowska 1999). However, Böckmann et al. (2008) extracted a linear form of  $f(E)$  from pore formation simulations. Semi-logarithmic plots of initiation time versus  $E$  from our simulations (Fig. 4b) show nonlinearity for both POPC and WVW systems. We suggest that a determination of the exact form of  $f(E)$  is premature at this stage due to the large statistical variation in the initiation time. A more reliable extraction of  $f(E)$  would require a more extensive statistical and energetic study.

We examined the initiation time of WVW systems with two different gap thicknesses: 2.8 nm, which yields an internal versus external field relationship similar to POPC systems, and 4.0 nm, which is approximately the distance between top and bottom water groups in POPC systems. Since the energy barrier between the water groups increases with the vacuum gap size, the field required to initiate a water bridge in a given time is much larger for WVW systems with a 4.0 nm gap than for those with a 2.8 nm gap. Intuitively we expect that it is easier to drive water molecules across a vacuum gap than across the interior of a

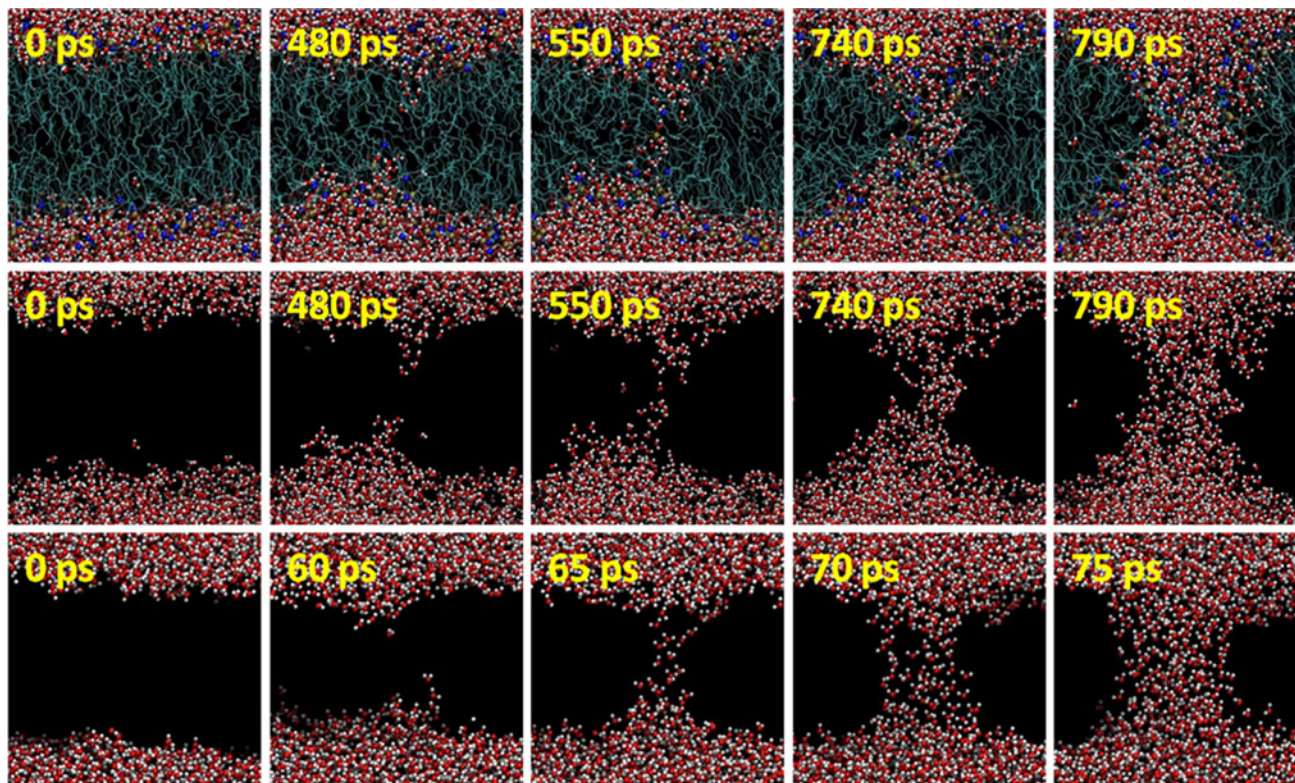


**Fig. 3** Water bridge formation in POPC (*top and middle row*) and WVW (*bottom row*) systems. Water hydrogen and oxygen atoms are *white spheres* and *red spheres*, respectively. In the *top row*, nitrogen atoms and phosphorus atoms of POPC headgroups are *blue spheres*

and *gold spheres*, and lipid tails are represented as *light blue lines*. The *frames* in the *middle row* are identical to those in the *top row*, except that only water molecules are displayed

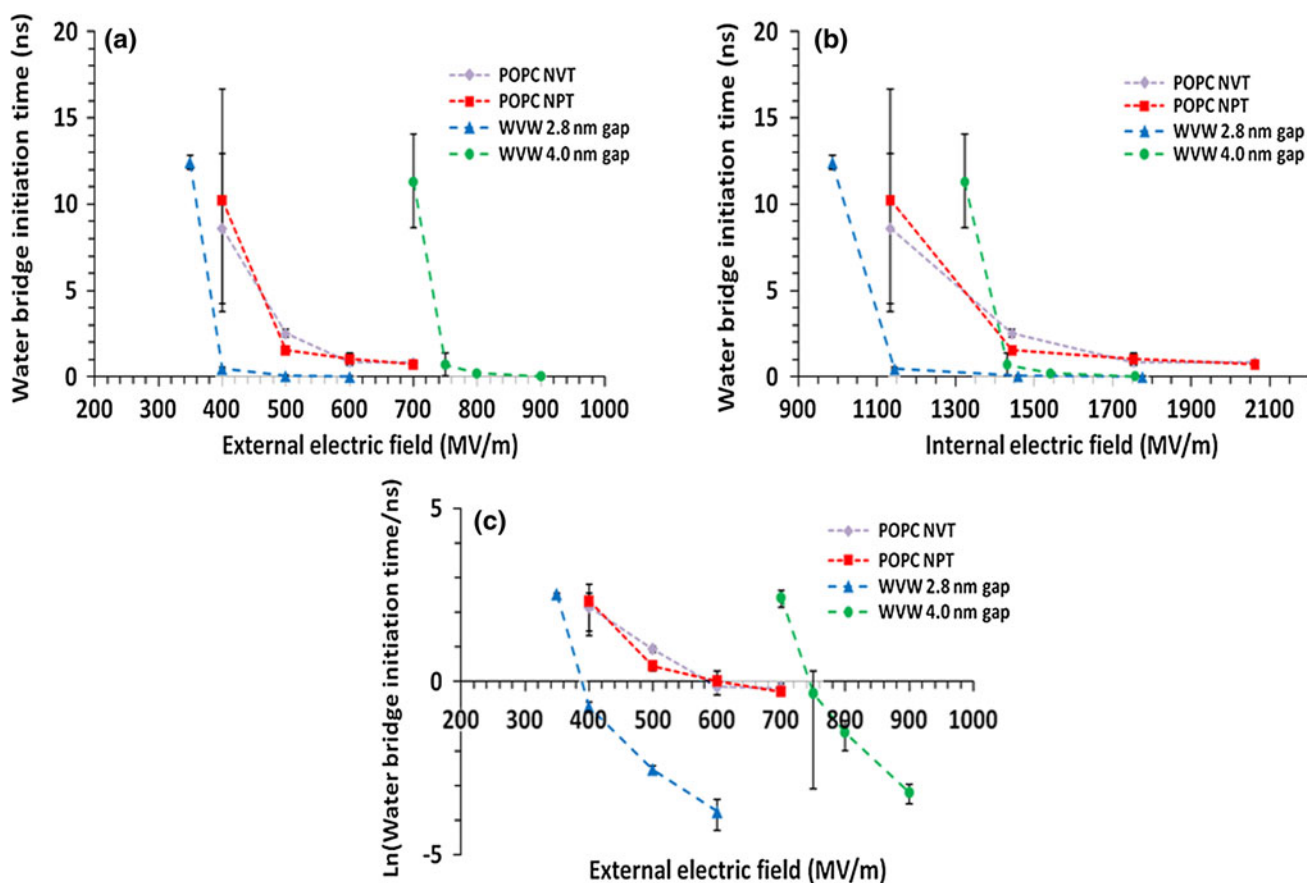


**Fig. 4** **a** Water bridge initiation time versus external electric field strength. **b** Water bridge initiation time versus internal electric field strength, **c** Semilogarithmic plot of water bridge initiation time versus

external electric field strength. Each data point is the average of 3 simulations. *Error bars* are the standard deviation

lipid bilayer, and we see this in the shorter initiation times for WWV systems compared to POPC systems with similar internal electric field.

No characteristic prebridge restructuring of water molecules following the application of the external field and preceding the initial water intrusion that leads to bridge formation has yet been identified. Extension of the chain of water molecules into the lipid/vacuum region is very fast once it begins. At the lowest field strength we examined ( $350 \text{ MV m}^{-1}$ ), the intrusion time of water molecules into the lipid/vacuum region is in general less than 500 ps, while the total initiation time can be more than 10 ns. Although we have not yet developed efficient protocols for analytically characterizing water intrusions, the growth of water intrusions appears to be faster with higher electric fields, based on inspection of the simulation trajectories. Water intrusion times in WWV system are much shorter than in POPC systems ( $\sim 10$  vs.  $\sim 100$  ps), suggesting that the fatty acid chains of the lipid bilayer behave as a mechanical barrier that slows down the construction of the water bridge.

Water bridge formation can be observed by monitoring the water dipole moment (Fig. 5). In the absence of an external electric field, water molecules are ordered locally by hydrogen bonding and head group electrostatic interactions, and the system has a zero net dipole moment. Application of an external field orients the water dipoles, producing a finite net dipole moment in the system. The system dipole moment increases again when the water bridge is formed (indicated by the red lines in Fig. 5). The net dipole moment increases rapidly during the expansion of the water bridge.

Recall from basic electromagnetics that when two dipoles are placed parallel to each other with the same orientation, their dipole–dipole interaction energy is positive. In our simulations, the water dipoles are forced to align in the  $z$  direction by the external field. In order to minimize the potential energy, the system favors the extension of water intrusions in the  $z$  direction and the lengthening of the growing water bridge, which increases the surface area parallel to the  $z$  direction and reduces the number of parallel dipole neighbors.

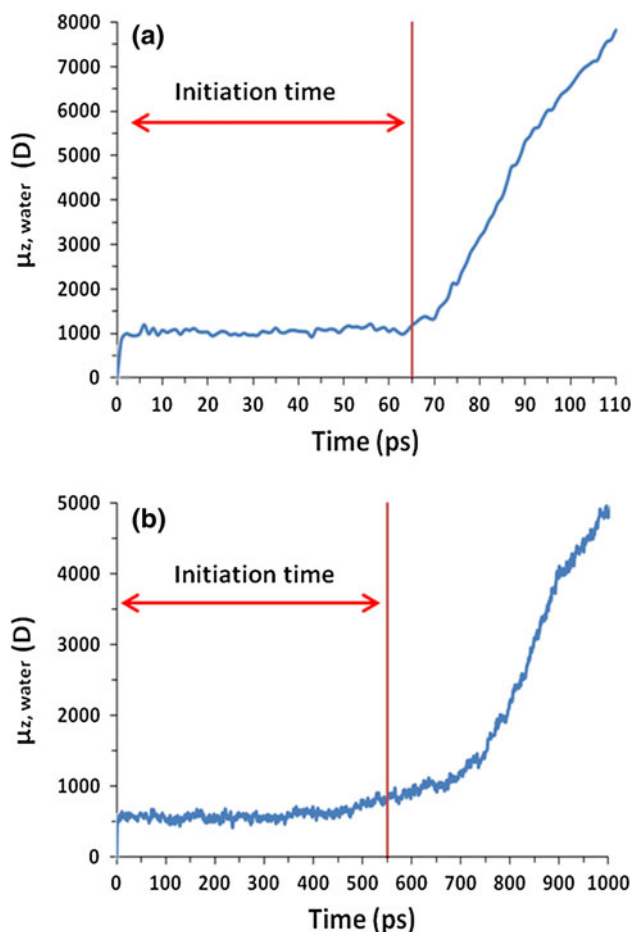


**Fig. 5** Total system dipole moment of water in  $z$  direction vs. time during water bridge formation from selected simulations in **a** WWV and **b** POPC systems. The external field is applied at  $t = 0$ . *Top and bottom water groups connect at the time indicated by the red lines*

### Water Bridge Stabilization

To simplify the discussion, we consider here only the water bridge and subsequent water column that forms in either POPC or WWV systems. A sufficiently large electric field ( $>300 \text{ MV m}^{-1}$ ) is required to create a water bridge within a reasonable simulation time ( $<25 \text{ ns}$ ) (Ziegler and Vernier 2008). If this field continues to be applied after the water bridge forms, the water column expands radially until anomalies arising from finite size effects appear.

If, however, the external field is reduced after the water bridge forms, the bridge can be stabilized with a constant radius, similar to what has been reported previously for phospholipid bilayers (Fernández et al. 2012). In our simulations, a water bridge can be stabilized with sustaining fields ranging from 50 to  $100 \text{ MV m}^{-1}$  in both POPC and WWV systems. (Note that this range is similar to that observed in lipid bilayer systems (Fernández et al. 2012). Within this range, the stabilized, time-averaged water bridge radius increases roughly linearly with the sustaining

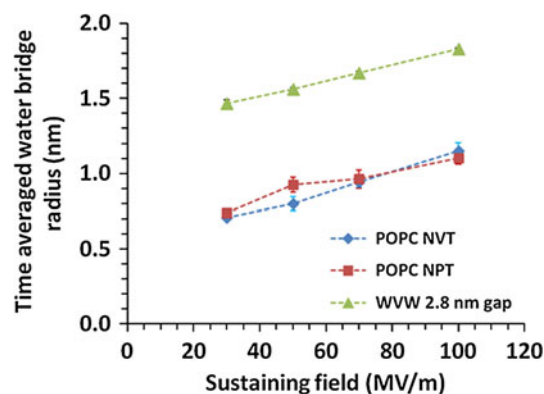


**Fig. 6** Time-averaged water bridge radius versus sustaining field. Time-averaged values were obtained from 20 ns trajectories after equilibration. Each data point is the average of 3 simulations. *Error bars are the standard deviation*

field for both POPC and WWV systems. But without the constraining presence of the phospholipid pore wall, the water bridge radius in WWV systems is larger for a given sustaining field than the corresponding structure in POPC systems (Fig. 6). If the sustaining field is greater than  $150 \text{ MV m}^{-1}$ , the water bridge expands in both systems until finite size defects emerge.

In continuum models of electroporation, the stabilized state of an electropore is predicted since the strength of the external field modifies the energy landscape of the membrane and creates an energy minimum in the corresponding pore radius space (Neu and Krassowska 1999). Due to the nanoscale dimensions of these electropores, a method for direct observation of a stabilized electropore has not been developed, and it is difficult to achieve direct comparisons with model predictions. However, some macroscopic measurements, such as conductance of charged molecules through the membrane (Koronkiewicz et al. 2002), can serve as indirect comparisons for validating the predictions of microscopic simulations and continuum models.

POPC and WWV systems differ in the time required for a system to evolve to a new equilibrium after the external field is reduced. Figure 7 shows the evolution of the water bridge radius under various sustaining fields. The water bridge radius in WWV systems reaches an equilibrium value in a few 100 ps or less after the external field is reduced. POPC systems take several nanoseconds to stabilize. This difference in the kinetics of water bridge radius evolution is probably a consequence of the momentum and interactions of the lipids in the pore wall of the POPC systems, which hinders water bridge expansion and contraction.

### Water Bridge Annihilation

When the external electric field is removed, water molecules in the system are no longer preferentially oriented in

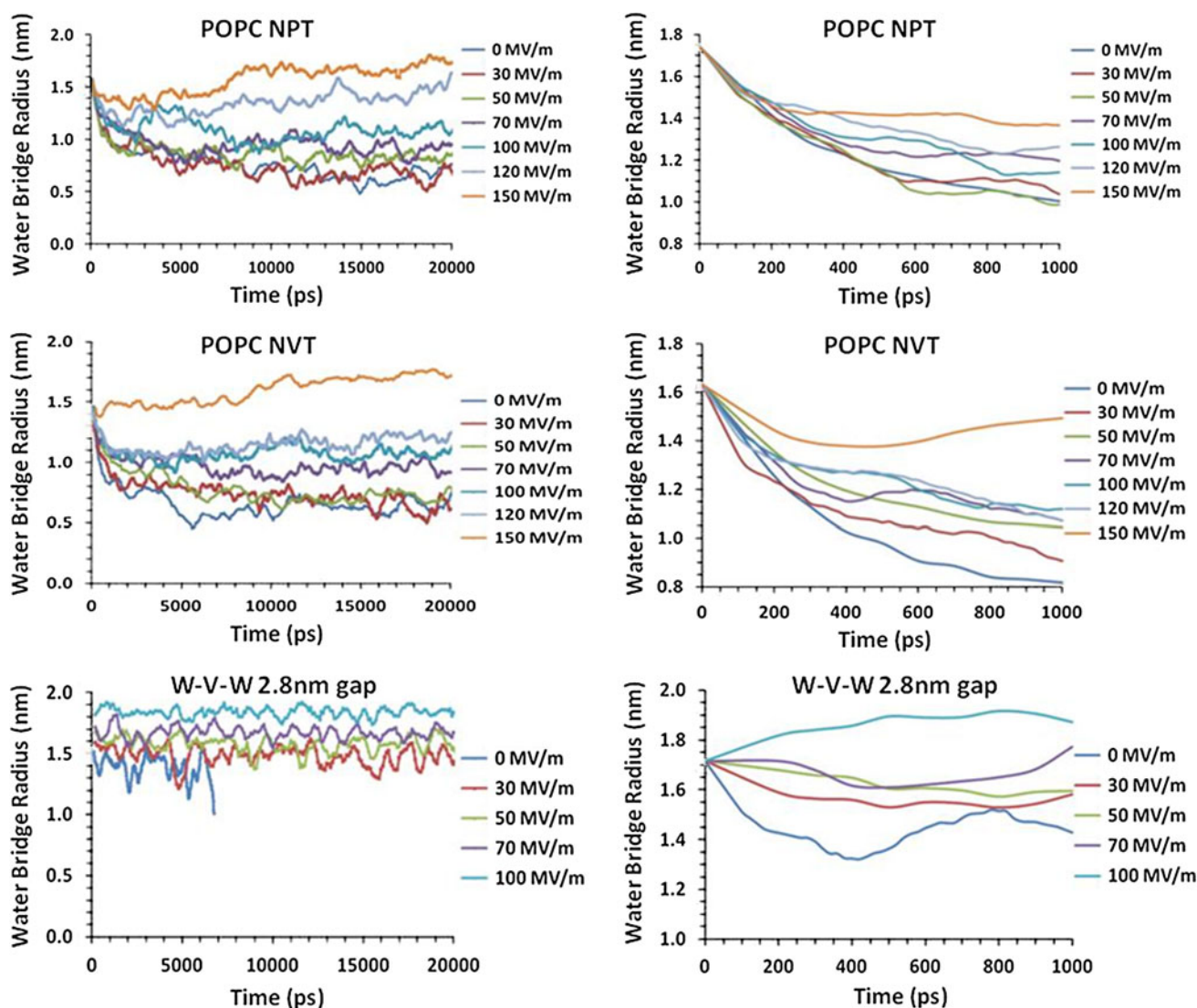


**Fig. 7** Evolution of water bridge radius during stabilization from selected simulations. At  $t = 0$ , the external field was reduced to the sustaining field value in the legend. The plots were smoothed using moving averaging of 10 time frames

the  $z$  direction, and the water bridge becomes an energetically unfavorable configuration. Hydrogen bond associations drive the migration of water molecules back into the bulk, and the bridge is annihilated. In POPC systems, the deconstruction of the water bridge involves also the hydrophilic interactions between water and the phospholipid head groups in the pore wall, as the pore lipids move back into the plane of the bilayer.

Figure 8 shows how the water bridge annihilation time (defined as the time between the removal of the field and the disconnection of the top and bottom water groups) varies with the radius of the water column when the field is removed. In WVV systems the water bridge collapses very quickly ( $<0.3$  ns) when the initial bridge radius is less than 1.2 nm. Water bridges with radii larger than 1.2 nm are stable for

about 10 ns before annihilation, and the annihilation time is independent of bridge radius for values up to 2.0 nm.

In contrast with WVV systems, annihilation time in POPC systems is dependent on bridge radius. Annihilation of a phospholipid membrane pore involves the rearrangement of both water and lipids. Since larger pores incorporate more lipids which must move back into the bilayer, it is not surprising that water bridge annihilation times are much longer in POPC systems than they are in WVV systems. We can conclude that the dynamics of electropore annihilation in phospholipid bilayers are determined primarily by the properties of the lipids, and that the lifetime of the water bridge in a POPC system is extended by the hydrophilic interaction between the bridge water and the pore lipids.

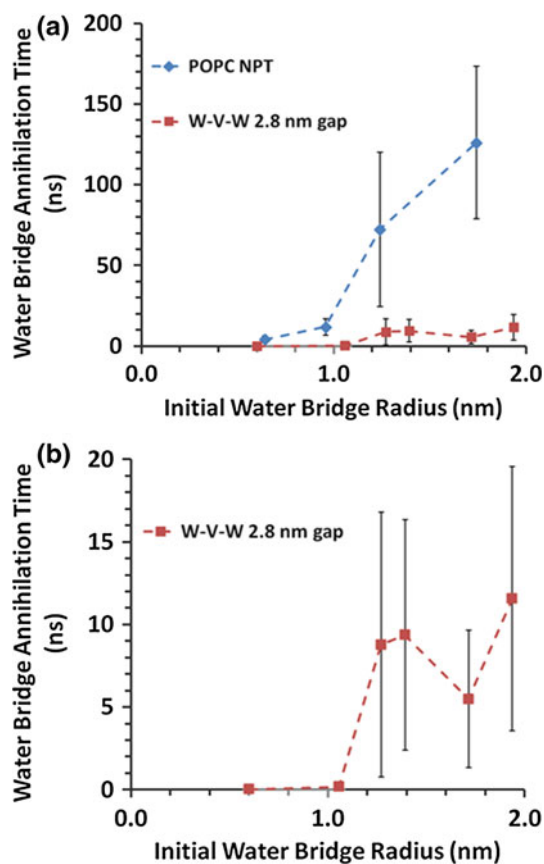


**Fig. 8** **a** Water bridge annihilation time versus initial water bridge radius for POPC and WWV systems. **b** Same WWV data plotted with an expanded vertical axis. Each data point is the average of at least 3 simulations. *Error bars* are the standard deviation

## Summary

We performed MD simulations to study the water bridge in WWV and POPC systems during different stages of electropore formation in order to delineate the roles of water and lipids. The dynamics of water bridge formation in both systems are similar, and both systems exhibit an exponential decrease in water bridge initiation time with increasing external electric field.

Once a water bridge has formed, the radius of the bridge in both POPC and WWV systems increases roughly linearly with the magnitude of the sustaining electric field over the range of values we examined. For a given value of the sustaining field, the radius of the water bridge is larger in a WWV system than in a POPC system. Changes in bridge radius in response to changes in applied electric field are faster in WWV systems than in POPC systems.

Annihilation of the water bridge occurs much faster in a WWV system than in a POPC system. Water bridge annihilation time does not increase with the radius when the radius is above 1.2 nm in WWV systems, but it increases significantly with the radius in POPC systems,

suggesting that hydrophilic interactions between the water and the lipid pore wall and among the pore lipids themselves contribute to the stabilization of a phospholipid electropore, and that the properties of the lipids are key determinants of the stability of the electropore.

## References

- Berendsen HJC, Postma JPM, van Gunsteren WF (1981) Interaction models for water in relation to protein hydration. In: Pullman B (ed) *Intermolecular forces*. Reidel, Dordrecht, pp 331–342
- Berendsen HJC, Postma JPM, van Gunsteren WF et al (1984) Molecular dynamics with coupling to an external bath. *J Chem Phys* 81:3684–3690
- Berger O, Edholm O, Jahnig F (1997) Molecular dynamics simulations of a fluid bilayer of dipalmitoylphosphatidylcholine at full hydration, constant pressure, and constant temperature. *Biophys J* 72:2002–2013
- Böckmann RA, de Groot BL, Kakorin S et al (2008) Kinetics, statistics, and energetics of lipid membrane electroporation studied by molecular dynamics simulations. *Biophys J* 95:1837–1850
- Bussi G, Donadio D, Parrinello M (2007) Canonical sampling through velocity rescaling. *J Chem Phys* 126:014101
- DeBruin KA, Krassowska W (1999) Modeling electroporation in a single cell. I. Effects of field strength and rest potential. *Biophys J* 77:1213–1224
- Essmann U, Perera L, Berkowitz MD et al (1995) A smooth particle mesh Ewald method. *J Chem Phys* 103:8577–8593
- Fernández ML, Marshall G, Sagués F et al (2010) Structural and kinetic molecular dynamics study of electroporation in cholesterol-containing bilayers. *J Phys Chem B* 114:6855–6865
- Fernández ML, Risk M, Reigada R et al (2012) Size-controlled nanopores in lipid membranes with stabilizing electric fields. *Biochem Biophys Res Commun* 423:325–330
- Heller LC, Heller R (2006) In vivo electroporation for gene therapy. *Hum Gene Ther* 17:890–897
- Hess B, Bekker H, Berendsen HJC et al (1997) LINCS: a linear constraint solver for molecular simulations. *J Comput Chem* 18:1463–1472
- Hess B, Kutzner C, van der Spoel D et al (2008) GROMACS 4: algorithms for highly efficient, load-balanced, and scalable molecular simulation. *J Chem Theory Comput* 4:435–447
- Humphrey W, Dalke A, Schulten K (1996) VMD: visual molecular dynamics. *J Mol Graph* 14:33–38
- Koronkiewicz S, Kalinowski S, Bryl K (2002) Programmable chronopotentiometry as a tool for the study of electroporation and resealing of pores in bilayer lipid membranes. *Biochim Biophys Acta* 1561:222–229
- Krassowska W, Filev PD (2007) Modeling electroporation in a single cell. *Biophys J* 92:404–417
- Levine ZA, Vernier PT (2010) Life cycle of an electropore: field-dependent and field-independent steps in pore creation and annihilation. *J Membr Biol* 236:27–36
- Levine ZA, Vernier PT (2012) Calcium and phosphatidylserine inhibit lipid electropore formation and reduce pore lifetime. *J Membr Biol* 245:599–610
- Mir LM, Morsli N, Garbay JR et al (2003) Electrochemotherapy: a new treatment of solid tumors. *J Exp Clin Cancer Res* 22(4 Suppl):145–148
- Miyamoto S, Kollman PA (1992) SETTLE: an analytical version of the SHAKE and RATTLE algorithm for rigid water models. *J Comput Chem* 13:952–962



- Neu JC, Krassowska W (1999) Asymptotic model of electroporation. *Phy Rev E* 59:3471–3482
- Neumann E, Schaefer-Ridder M, Wang Y et al (1982) Gene transfer into mouse lymphoma cells by electroporation in high electric fields. *EMBO J* 1:841–845
- Okuno Y, Minagawa M, Matsumoto H et al (2009) Simulation study on the influence of an electric field on water evaporation. *J Mol Struct (Theochem)* 904:83–90
- Piggot TJ, Holdbrook DA, Khalid S (2011) Electroporation of the *E. coli* and *S. aureus* membranes: molecular dynamics simulations of complex bacterial membranes. *J Phys Chem B* 115:13381–13388
- Tarek M (2005) Membrane electroporation: a molecular dynamics simulation. *Biophys J* 88:4045–4053
- Teissie J, Golzio M, Rols MP (2005) Mechanisms of cell membrane electroporation: a minireview of our present (lack of?) knowledge. *Biochim Biophys Acta* 1724:270–280
- Tieleman DP (2004) The molecular basis of electroporation. *BMC Biochem* 5:10
- Vernier PT, Ziegler MJ (2007) Nanosecond field alignment of head group and water dipoles in electroporating phospholipid bilayers. *J Phys Chem B* 111:12993–12996
- Vernier PT, Levine ZA, Gundersen MA (2013) Water bridges in electroporation of phospholipid bilayers. *Proc IEEE* 101:494–504
- Weaver JC, Chizmadzhev YA (1996) Theory of electroporation: a review. *Bioelectrochem Bioenerg* 41:135–160
- Ziegler MJ, Vernier PT (2008) Interface water dynamics and porating electric fields for phospholipid bilayers. *J Phys Chem B* 112:13588–13596
- Zimmermann U, Pilwat G, Riemann F (1974) Dielectric breakdown of cell membranes. *Biophys J* 14:881–899